OET | Opto-Electronic Technology

CN 51-1811/O4 ISSN (Print) 2097-6003

Non-volatile reconfigurable planar lightwave circuit splitter enabled by laser-directed Sb_2S_3 phase transitions

Shixin Gao, Tun Cao, Haonan Ren, Jingzhe Pang, Ran Chen, Yang Ren, Zhenqing Zhao, Xiaoming Chen and Dongming Guo

Citation: Gao SX, Cao T, Ren HN, et al. Non-volatile reconfigurable planar lightwave circuit splitter enabled by laser-directed Sb_2S_3 phase transitions. *Opto-Electronic Technology* **1**, 250002(2025).

https://doi.org/10.29026/oet.2025.250002

Received: 31 May 2025; Accepted: 4 July 2025; Published online: 8 July 2025

OET | Opto-Electronic Technology
www.oejournal.org/oet

Article
July 2025, Vol. 1, No. 1

DOI: 10.29026/oet.2025.250002 | CSTR: 32419.14.oet.2025.250002

Open Access

Non-volatile reconfigurable planar lightwave circuit splitter enabled by laser-directed Sb_2S_3 phase transitions

Shixin Gao[1†], Tun Cao[1*†], Haonan Ren[1], Jingzhe Pang[1], Ran Chen[1], Yang Ren[3], Zhenqing Zhao[4], Xiaoming Chen[1] and Dongming Guo[2*]

Abstract: Planar lightwave circuit (PLC) splitters have long been foundational components in passive optical communication networks, achieving commercial success since the 1990s. However, their inherent fixed splitting ratios impose significant limitations on capacity expansion, often requiring physical replacement and causing service disruptions. Thermally tunable optical splitters address this challenge by enabling adjustable splitting ratios, but their operation is contingent upon a continuous power supply and complex driving systems. In this work, we present a novel, non-volatile tunable PLC platform based on Sb_2S_3 phase-change materials. The proposed device, which incorporates a Mach-Zehnder interferometer (MZI) optical switch structure, offers tunable splitting ratios via laser-direct writing or ohmic heating, providing flexible reconfiguration capabilities. Experimental results demonstrate non-volatile power splitting ranging from 50∶50 to 20∶80, with a modest increase of approximately 1 dB in additional loss. This work highlights the potential of the proposed platform for low-power, high-efficiency, and reconfigurable photonic networks.

Keywords: phase change materials; reconfigurable; planar lightwave circuit; integrated photonic devices; optical routing

Introduction

Passive optical networks (PONs) have become increasingly essential as global broadband demand surges, driven by the need for high-speed connectivity[1–3]. Planar lightwave circuits (PLCs) are fundamental components in PON networks, playing a pivotal role in enabling efficient and low-cost optical communication solutions[4–6]. These splitters are commonly designed with Y-branch waveguide structures, supporting from 2 to 128 or more channels to meet the diverse requirements of modern optical communication systems[7–11]. Key performance metrics for PLC splitters include low insertion loss, customizable splitting ratios, a wide operating wavelength range, and a compact, low-cost design. However, as passive components, the fixed splitting ratios of conventional PLC splitters severely limit network flexibility. For instance, capacity expansion requires the physical replacement of these devices, inevitably causing service interruptions.

While Mach-Zehnder interferometer (MZI)-based tunable splitters using thermo-optic effects have been developed to address this limitation, their non-volatile operation demands continuous power to maintain configurations, leading to high energy consumption[12,13]. Furthermore, the integration of microheaters introduces fabrication complexities, such as additional lithographic and etching steps for electrical interconnects, which increase costs and conflict with the cost-sensitive manufacturing paradigm of PLCs.

Phase-change materials (PCMs) have emerged as a novel solution for non-volatile reconfigurable photonic devices, overcoming the limitations of volatile tuning mechanisms[14]. PCMs enable reversible switching between amorphous and crystalline states through controlled heating and quenching processes, leveraging the significant refractive index contrast between these phases to create compact and efficient photonic devices. Early PCMs, such as $Ge_2Sb_2Te_5$ (GST), have demonstrated promising applications in tunable metasurfaces[15–17], non-volatile photonic

Received: 31 May 2025
Accepted: 4 July 2025
Published online: 8 July 2025

[1]School of Optoelectronic Engineering and Instrumentation Science, Dalian University of Technology, Dalian 116024, China; [2]Key Laboratory for Precision and Non-traditional Machining Technology of Ministry of Education, Dalian University of Technology, Dalian 116024, China; [3]Huawei Technologies, B & P Laboratory, Shenzhen 518000, China; [4]Huawei Technologies, Optical R & D Dept. Dongguan 523808, China.
[†]These authors contributed equally to this work.
*Correspondence: T Cao, E-mail: caotun1806@dlut.edu.cn; DM Guo, E-mail: guodm@dlut.edu.cn

memories[18–20], and reconfigurable optical neural networks[21–23]. However, their high optical loss in the telecommunication band has limited their practical use in low-loss photonic circuits.

Recently, a new class of low-loss PCMs, particularly antimony trisulfide (Sb_2S_3), has gained considerable attention due to its exceptional properties[24–26]. Sb_2S_3 exhibits a wide transparency range from visible to near-infrared wavelengths, with a refractive index contrast of approximately 0.6 between its amorphous and crystalline states. Combined with its low optical loss and excellent thermal stability, Sb_2S_3 has become a leading candidate for reconfigurable photonic applications. Notably, laser-induced phase transitions in Sb_2S_3 have enabled etching-free reconfigurable waveguides on platforms such as silicon nitride and silicon-on-insulator (SOI), demonstrating ultra-low absorption loss and paving the way for high-performance, low-loss photonic devices[27–29]. These advancements highlight the potential of Sb_2S_3 for enabling next-generation programmable photonic circuits with non-volatile operation.

This work demonstrates a novel approach to realizing non-volatile tunable PLC splitters through the integration of Sb_2S_3 with commercial PLC platforms. The laser-induced crystallization process enables precise regional phase shift control through optimized amorphous-to-crystalline phase transitions. Critical process parameters, including laser power, scanning speed, and crystallization patterns, were systematically explored to achieve the optimal crystallization state. By incorporating laser-direct-written Sb_2S_3 phase shifters in an MZI configuration, we achieved a wide splitting ratio adjustment range from 50∶50 to 20∶80, with an additional insertion loss of approximately 1 dB. This work demonstrates a reconfigurable PLC splitter that expands the functionality and performance of PLCs, offering a low-cost, low-energy solution for intelligent optical communication networks.

Results and discussions

Principle of operation

The central concept of this work exploits the refractive index contrast of Sb_2S_3 thin films between their amorphous (n = 2.7) and crystalline (n = 3.3) states to create a phase shifter integrated into an MZI structure on a PLC platform. This setup enables reconfigurable splitting ratios. The phase shift induced by the transition of Sb_2S_3 from the amorphous to crystalline state alters the interference conditions within the MZI arms, allowing precise control over the splitting ratio. The phase shifter consists of a PCM-modified PLC waveguide, as illustrated in Fig. 1(a). It features a thin Sb_2S_3 layer coated on the waveguide surface, protected by an oxide capping layer. Localized crystallization is induced by laser writing (> 270 °C) on one MZI arm, creating a phase difference proportional to the written length. This is demonstrated in the inset of Fig. 1(a), where the output light spots from the PLC waveguide are captured through a low-magnification lens and imaged on an infrared camera (Supplementary information Fig. S1). The phase shift resulting from laser writing inverts the output intensity ratio between ports A and B. The sample shown is a commercially fabricated PLC waveguide with the top cladding removed, as shown in Fig. 1(b), and includes alignment fixtures for fiber array (FA) packaging. The waveguide structure is visible in the microscope image of Fig. 1(c), where the brown regions correspond to the deposited Sb_2S_3 layer. The fabrication process has been schematically shown in Supplementary information Fig. S2.

The structure of the PCM-modified PLC waveguide is shown in Fig. 1(d). The core width (w = 6.7 μm) and core-to-surface distance (h) facilitate partial evanescent field interaction with the Sb_2S_3 layer. This relatively thick layer compensates for the weak evanescent field overlap in large-core waveguides, allowing for practical phase-shift lengths. Figure 1(e) illustrates the calculated modal field distribution in the phase-shifter region. Numerical simulations reveal polarization-dependent behavior due to the asymmetric placement of Sb_2S_3. The transverse magnetic (TM) mode shows stronger field overlap with the Sb_2S_3 layer (Fig. 1(e)), resulting in higher sensitivity to index changes but also increased coupling loss. The transverse electric (TE) mode exhibits weaker field overlap with the Sb_2S_3 layer, attributed to its reduced sensitivity to refractive index changes. Material losses, derived from the imaginary refractive index (k_c = 0.0001 for crystalline, k_a = 0 for amorphous), contribute minimal losses in both the crystalline and amorphous states[30]. For unpolarized light inputs, the extinction ratio between the two ports is limited to 18.5 dB, as unpolarized light contains an equal mix of TE-mode light, which cannot produce effective interference due to insufficient phase accumulation. Extending this range will require polarization-insensitive designs, such as symmetric Sb_2S_3 coating on both sides of the waveguide, representing a potential direction for future research.

Laser direct writing of large-area crystalline Sb_2S_3

Compared to conventional annealing methods using a hotplate or microheater, laser direct writing achieves superior crystallization uniformity (Supplementary information Fig. S3), with larger grain sizes and reduced boundary density, effectively mitigating optical losses[28,30]. High-quality Sb_2S_3 crystallization requires precise control of laser writing parameters, which significantly influence both crystallinity and optical loss. To systematically investigate laser-induced phase transitions, we used silica microscope slides coated with 300 nm of amorphous Sb_2S_3 and 50 nm Al_2O_3 capping layers (fabricated via electron-beam evaporation) as test platforms, taking advantage of their physical similarity to PLC substrates. A combinatorial parameter study was conducted using a custom-built laser writing system, varying scanning speeds (10, 20, 40, and 100 μm/s) and laser

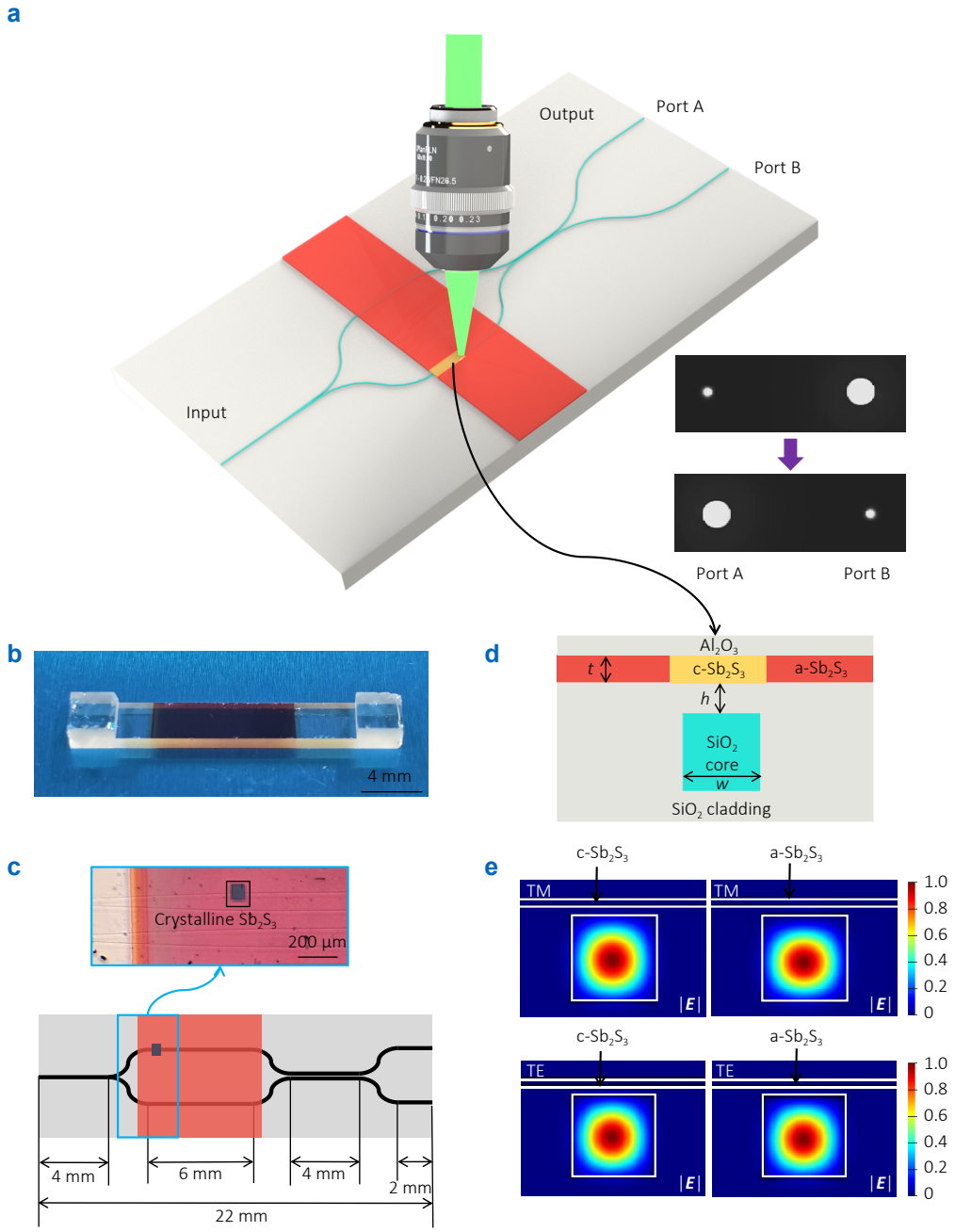

Fig. 1 | (**a**) Schematic diagram of the laser direct-writing process for the tunable PLC splitter. Inset: near-infrared microscopic image of the output light spots at ports A and B of the splitter, captured before and after laser writing of 3 mm. (**b**) Photograph of the tunable PLC splitter, with the brown color regions indicating the deposited Sb_2S_3 layer. (**c**) The overall architecture of the PLC with critical dimensions annotated at key locations, where the blue rectangle demarcates the region subjected to microscopic imaging of the PCM-modified waveguide, and the black rectangle identifies the laser-direct-written crystallization zone. (**d**) Cross-section of the PCM-modified PLC region, with key geometric parameters annotated: *t* (Sb_2S_3 thin film thickness), *h* (gap height between Sb_2S_3 and PLC core region), and *w* (PLC core width). (**e**) Comparison between the PCM-modified region without laser writing and the PCM-modified region after laser writing.

powers (2, 3, 5, and 8 mW), as shown in Fig. 2(a).

At suboptimal 2 mW power, incomplete crystallization resulted in narrow, shallow traces with a mixture of amorphous and crystalline phases. In contrast, excessive 8 mW power caused localized overheating and film delamination at the Sb_2S_3/Al_2O_3 interface. Crystallographic texture analysis revealed that grain structure alignment strongly depends on the scanning trajectories (Fig. 2(b)). Unidirectional scanning at 20 μm/s produced aligned grain structures along the writing axis, while complex patterns, such as spiral and S-shaped fillings, led to disordered grain boundaries. This outcome is due to directional grain growth

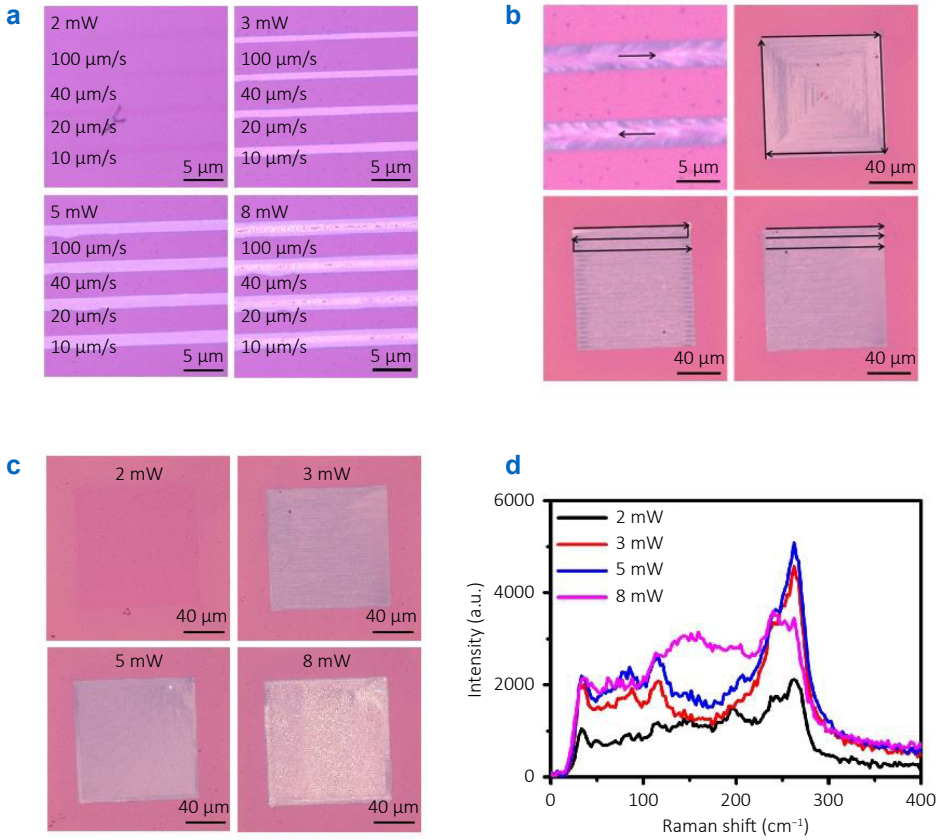

Fig. 2 | (**a**) Microscope images of Sb_2S_3 thin films fabricated by laser direct writing at different scanning rates (10–100 μm/s) and laser powers (2–8 mW). (**b**) Polarized microscope images of Sb_2S_3 thin films with different writing directions and filling methods. (**c**) The crystalline morphology of Sb_2S_3 thin films prepared by direct writing at different powers. (**d**) Raman spectra of the central regions in (c).

being influenced by the laser scanning speed relative to the intrinsic crystallization growth kinetics.

Power-dependent crystallization dynamics were further analyzed through Raman spectroscopy. Direct-write filling was performed on the samples using laser powers of 2, 3, 5, and 8 mW at a scanning speed of 100 μm/s, as shown in Fig. 2(c, d). Optimal crystallinity, indicated by distinct Raman peaks at 189 cm^{-1} and 290 cm^{-1}, occurred in the 3–5 mW range. Subthreshold 2 mW irradiation preserved the amorphous-phase spectral signatures, while 8 mW exposure resulted in material degradation, with attenuated Raman peaks.

These experiments revealed that power and scanning speed are interdependent parameters. Within an optimal range, such as a scanning speed of 10–40 μm/s combined with power settings of 3–5 mW, uniform planar crystallization can be achieved. While higher power and faster scanning speeds may improve production efficiency, if the scanning speed exceeds the crystallization growth rate by a significant margin, the crystallization dynamics change: instead of progressing along the scanning direction, crystallization occurs simultaneously across the heated region[31]. This can result in discontinuous crystallization growth, smaller grain sizes, and higher transmission losses. Therefore, careful optimization of both power and scanning speed is crucial for achieving stable and high-quality crystallization[32–34].

Transmission characterization

We systematically investigated the optical transmission characteristics of a PCM-modified PLC waveguide phase shifter integrated into an MZI splitter. To optimize performance, we analyzed the phase shift dependence on two critical parameters: the Sb_2S_3 layer thickness and the gap height (h) between the PLC waveguide and the Sb_2S_3 layer. Figure 3(a) shows the phase shift as a function of Sb_2S_3 thickness under fixed laser-writing conditions (6 mm writing length, h = 1 μm). A 500 nm Sb_2S_3 layer achieves a complete π-phase shift for the transverse magnetic (TM) mode, while weaker, but still measurable, phase modulation occurs in the transverse electric (TE) mode. Figure 3(b) further quantifies the interdependence of gap height (h), phase shift magnitude, and optical losses induced by the Sb_2S_3 state transformation (writing length: 6 mm, Sb_2S_3 thickness: 500 nm). Our simulations covered a range of gap heights from 450 nm to 950 nm to account for fabrication tolerances. Smaller gap heights enhance phase modulation by increasing the light-PCM interaction but may also lead to mode distortion and coupling losses between the PLC waveguide and the PCM-modified structure. Total losses

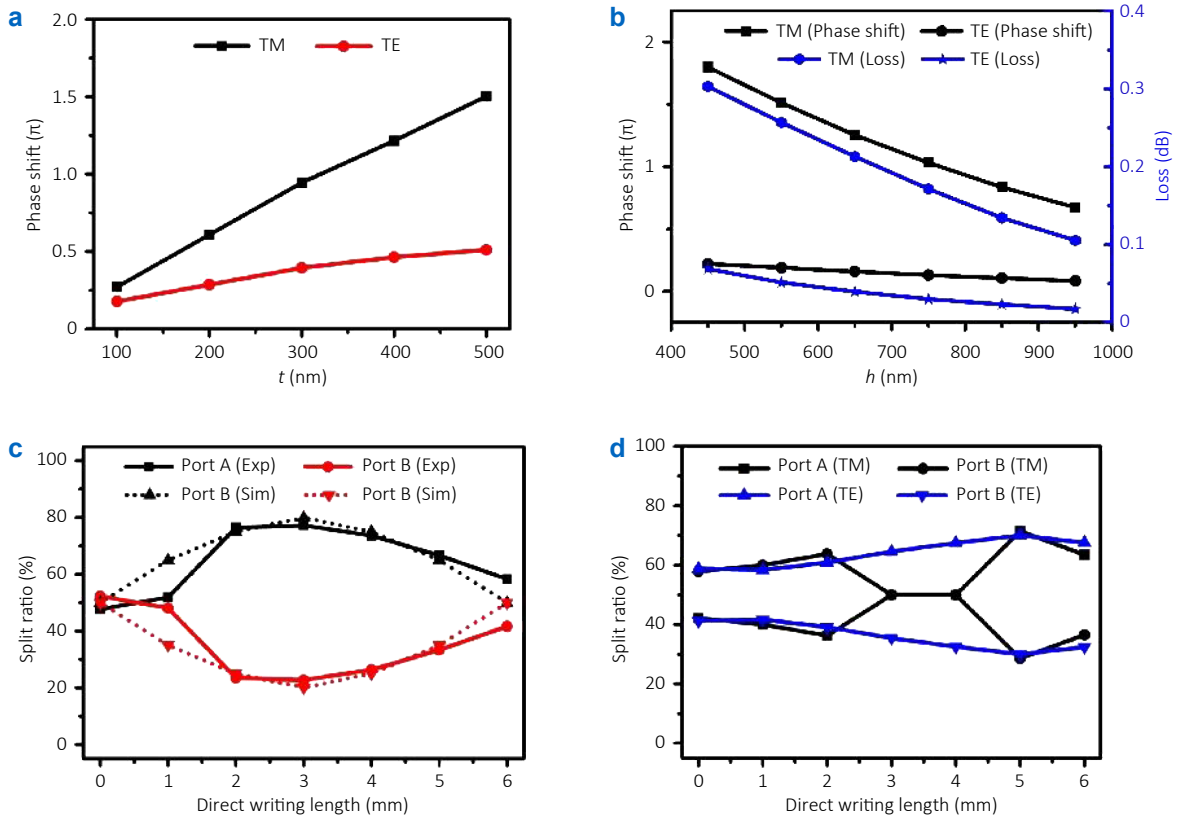

Fig. 3 | Optical performance of the PCM-modified PLC waveguide phase shifter integrated into an MZI splitter. (**a**) Phase shift as a function of Sb_2S_3 thickness under fixed laser-writing conditions (6 mm writing length, h = 1 μm). A 500 nm Sb_2S_3 layer achieves a complete π-phase shift for the TM mode, with weaker modulation observed for the TE mode. (**b**) Interdependence of gap height (h), phase shift magnitude, and optical losses. Simulations (h = 450–950 nm) reveal that a gap height below 750 nm is required for π-phase shift operation, with TM-mode absorption losses ranging from 0.0006 dB/mm to 0.0020 dB/mm. (**c**, **d**) Experimental validation of dynamic split ratio evolution in a fabricated PLC-MZI structure (h = 1 μm, 500 nm Sb_2S_3, 50 nm Al_2O_3). Laser modification (3 mm writing length) demonstrates split ratio tuning from 50 ∶ 50 to 80 ∶ 20, constrained by non-ideal directional coupler performance. Simulations indicate the feasibility of achieving 50 ∶ 50 to 1 ∶ 99 splitting ratio in optimized configurations.

arise from three mechanisms: intrinsic absorption in crystalline Sb_2S_3 (dominated by its extinction coefficient, k_c), scattering losses at polycrystalline grain boundaries (which are process-dependent), and mode coupling losses between the original PLC waveguide and the PCM-modified regions during phase transitions. Simulations reveal low TM-mode absorption losses (0.003 dB/mm–0.010 dB/mm). A gap height below 750 nm is required for π-phase shift operation, with theoretical insertion losses under 0.2 dB. Detailed calculations can be found in Supplementary information Fig. S4.

For experimental validation, we fabricated a custom PLC-MZI structure (h = 1 μm) with sequentially deposited 500 nm Sb_2S_3 and a 30 nm Al_2O_3 protection layer. Light was coupled through SMF-28 single-mode fibers, and the TE/TM mode splitting ratios were analyzed using a polarizer and power meter. The device exhibited an insertion loss of 2.9 dB before Sb_2S_3 deposition and 3.8 dB after deposition. The additional 0.9 dB loss is primarily attributed to two factors: mode mismatch between the original PLC waveguide and the Sb_2S_3-modified region, and fabrication process imperfections associated with the long deposition length (over 9 mm). The laser writing process introduced negligible additional loss, with the insertion loss increasing by only 0.2 dB after a 6 mm writing length on one arm of the MZI. Figure 3(c, d) compares the transmission spectra before and after laser writing with varying exposure lengths on one interferometer arm. The results demonstrate the dynamic evolution of the split ratio, transitioning from an initial 50 ∶ 50 balance to an 80 ∶ 20 ratio and subsequently returning to 60 ∶ 40. This performance is constrained by structural deviations in the output directional coupler, which exhibited a non-ideal 50 ∶ 50 split compared to design specifications. Notably, simulations suggest that 1 ∶ 99 splitting (18.5 dB extinction ratio) can be achieved in optimized configurations with minimized phase shifter losses. These results underscore the critical impact of directional coupler precision on MZI performance, a challenge we aim to address through PCM-based trimming techniques, implementing a validated methodology from silicon photonics platforms. Figure 3(d) reveals distinct polarization-dependent responses in the PLC splitter: as laser direct writing length increases from 0 mm to 6 mm, TE light shows a gradual shift from 40 ∶ 60 to 30 ∶ 70 splitting

ratio, while TM light undergoes pronounced cyclical variations —transitioning through 50∶50 and 30∶70 states before returning to 40∶60. This contrast confirms that TM mode achieves full phase modulation whereas TE mode attains only partial modulation, primarily due to TE's inherently weaker interaction with the phase-change material. The diminished modulation efficiency in TE mode originates from its significantly smaller effective refractive index contrast compared to TM mode, necessitating longer interaction lengths for equivalent phase control. The performance comparison of electrically reconfigurable non-volatile photonic devices based on phase change materials can be found in Supplementary information Table S1.

Conclusions

This work presents a non-volatile, reconfigurable PLC splitter, bridging the gap between conventional fixed-ratio devices and volatile tunable solutions. By leveraging the low-loss Sb_2S_3 on a commercial PLC platform, we achieve permanent splitting ratio tuning through laser-direct-written phase transitions in the MZI configuration. The Sb_2S_3-modified waveguide enables reversible switching of the splitting ratio from 50∶50 to 80∶20 with approximately 1 dB insertion loss. Theoretically, we verified an 18.5 dB extinction ratio and demonstrated polarization-dependent tunability, with performance limitations primarily attributed to directional coupler imperfections rather than the properties of the PCM. This architecture preserves standard PLC manufacturing workflows, requiring only a sputtering step and eliminating the need for additional lithography and etching processes. This novel platform offers a cost-effective solution for upgrading widely deployed passive optical networks, advancing the development of fully programmable PLC infrastructures.

References

1. Kim KS. On the evolution of PON-based FTTH solutions. *Inf Sci* **149**, 21–30 (2003).
2. Park SJ, Lee CH, Jeong KT et al. Fiber-to-the-home services based on wavelength-division-multiplexing passive optical network. *J Lightwave Technol* **22**, 2582–2591 (2004).
3. Lee CH, Sorin WV, Kim BY. Fiber to the home using a PON infrastructure. *J Lightwave Technol* **24**, 4568–4583 (2006).
4. Dougherty, J D. Advances in planar lightwave circuits. *OFC/NFOEC Technical Digest. Optical Fiber Communication Conference* **4**, 3(2005).
5. Himeno A, Kato K, Miya T. Silica-based planar lightwave circuits. *IEEE J Sel Top Quantum Electron* **4**, 913–924 (1998).
6. Honjo T, Inoue K, Takahashi H. Differential-phase-shift quantum key distribution experiment with a planar light-wave circuit Mach-Zehnder interferometer. *Opt Lett* **29**, 2797–2799 (2004).
7. Sakamaki Y, Saida T, Tamura M et al. Low-loss Y-branch waveguides designed by wavefront matching method and their application to a compact 1 × 32 splitter. *Electron Lett* **43**, 217–219 (2007).
8. Liu ZY, Yao WL, You MJ et al. Tantalum pentoxide integrated photonics: a promising platform for low-loss planar lightwave circuits with low thermo-optic coefficients. *ACS Photonics* **12**, 684–695 (2025).
9. Sakamaki Y, Saida T, Shibata T et al. Y-branch waveguides with stabilized splitting ratio designed by wavefront matching method. *IEEE Photonics Technol Lett* **18**, 817–819 (2006).
10. Fujisawa T, Yamashita Y, Sakamoto T et al. Scrambling-type three-mode PLC multiplexer based on cascaded Y-branch waveguide with integrated mode rotator. *J Lightwave Technol* **36**, 1985–1992 (2018).
11. Li C S, Li X, Qiu X Y et al. A novel planar waveguide super-multiple-channel optical power splitter. *J Lightwave Technol* **33**, 5019–5024 (2015).
12. Ding YZ, Yin YX, Guan BL et al. Mode-selective switch on silica-based PLC platform. *Opt Commun* **546**, 129757 (2023).
13. Zhang GW, Ding YY, Chen W et al. Polarization-insensitive interferometer based on a hybrid integrated planar light-wave circuit. *Photonics Res* **9**, 2176–2181 (2021).
14. Wuttig M, Bhaskaran H, Taubner T. Phase-change materials for non-volatile photonic applications. *Nat Photonics* **11**, 465–476 (2017).
15. Abdelraouf OAM, Anthur AP, Dong ZG et al. Multistate tuning of third harmonic generation in Fano-resonant hybrid dielectric metasurfaces. *Adv Funct Mater* **31**, 2104627 (2021).
16. Abdollahramezani S, Hemmatyar O, Taghinejad M et al. Electrically driven reprogrammable phase-change metasurface reaching 80% efficiency. *Nat Commun* **13**, 1696 (2022).
17. Zhang F, Xie X, Pu MB et al. Multistate switching of photonic angular momentum coupling in phase-change metadevices. *Adv Mater* **32**, 1908194 (2020).
18. Dong YD, Wu ZQ, Zhong WT et al. Optimized low-loss $Ge_2Sb_2Te_5$ superlattice: design, fabrication and application. *Adv Opt Mater* **13**, 2402092 (2025).
19. Pernice WHP, Bhaskaran H. Photonic non-volatile memories using phase change materials. *Appl Phys Lett* **101**, 171101 (2012).
20. Rios C, Hosseini P, Wright CD et al. On-chip photonic memory elements employing phase-change materials. *Adv Mater* **26**, 1372–1377 (2014).
21. Zhang CP, Wei ML, Zheng J et al. Nonvolatile multilevel switching of silicon photonic devices with In_2O_3/GST segmented structures. *Adv Opt Mater* **11**, 2202748 (2023).
22. Fang ZR, Chen R, Zheng JJ et al. Ultra-low-energy programmable non-volatile silicon photonics based on phase-change materials with graphene heaters. *Nat Nanotechnol* **17**, 842–848 (2022).
23. Tanriover I, Hadibrata W, Scheuer J et al. Neural networks enabled forward and inverse design of reconfigurable metasurfaces. *Opt Express* **29**, 27219–27227 (2021).
24. Delaney M, Zeimpekis I, Lawson D et al. A new family of ultralow loss reversible phase-change materials for photonic integrated circuits: Sb_2S_3 and Sb_2Se_3. *Adv Funct Mater* **30**, 2002447 (2020).
25. Laprais C, Zrounba C, Bouvier J et al. Reversible single-pulse laser-induced phase change of Sb_2S_3 thin films: multi-physics modeling and experimental demonstrations. *Adv Opt Mater* **12**, 2401204 (2024).
26. Liu HL, Dong WL, Wang H et al. Rewritable color nanoprints in antimony trisulfide films. *Sci Adv* **6**, eabb7171 (2020).
27. Delaney M, Zeimpekis I, Du H et al. Nonvolatile programmable silicon photonics using an ultralow-loss Sb_2Se_3 phase change material. *Sci Adv* **7**, eabg3500 (2021).
28. Wu CM, Deng HQ, Huang YS et al. Freeform direct-write and rewritable photonic integrated circuits in phase-change thin films. *Sci Adv* **10**, eadk1361 (2024).
29. Miller F, Chen R, Fröch J et al. Rewritable photonic integrated circuit canvas based on low-loss phase change material and nanosecond pulsed lasers. *Nano Lett* **24**, 6844–6849 (2024).
30. Gao SX, Ren HN, Pang JZ et al. Reconfigurable free form silicon photonics by phase change waveguides. *Adv Opt Mater* **13**, 2402997 (2025).
31. Franz Y. Polycrystalline silicon waveguides for integrated photonics (University of Southampton, Southampton, 2018).
32. Cui SY, Lu YY, Kong DP et al. Laser direct writing of Ga_2O_3/liquid

metal-based flexible humidity sensors. *Opto-Electron Adv* **6**, 220172 (2023).
33. Jiang QL, Chen L, Liu JK et al. Periodic transparent nanowires in ITO film fabricated via femtosecond laser direct writing. *Opto-Electron Sci* **2**, 220002 (2023).
34. Fu JC, Jiang MT, Wang Z et al. Supercritical metalens at h-line for high-resolution direct laser writing. *Opto-Electron Sci* **3**, 230035 (2024).

Acknowledgements

The work at Dalian University of Technology was sponsored by the National Key Research and Development Program of China (2020YFA0714504, 2019YFA0709100), the program of the National Natural Science Foundation of China (U24A20309, 62305043).

Author contributions

Tun Cao and Shixin Gao are equally contributed. Shixin Gao performed the major experimental work and device characterizations. Haonan Ren and Xiaoming Chen conceived the experimental design. Jingzhe Pang and Ran Chen supported experiments and data analysis. Yang Ren engineered the PLC MZI optical architecture. Zhenqing Zhao defined the industrial application requirements. Tun Cao supervised the project, established the research platform and co-authored the manuscript. Dongming Guo has guided the research direction.

Competing interests

The authors declare no competing financial interests.

Supplementary information

Supplementary information for this paper is available at
https://doi.org/10.29026/oet.2025.250002